

PAPER • OPEN ACCESS

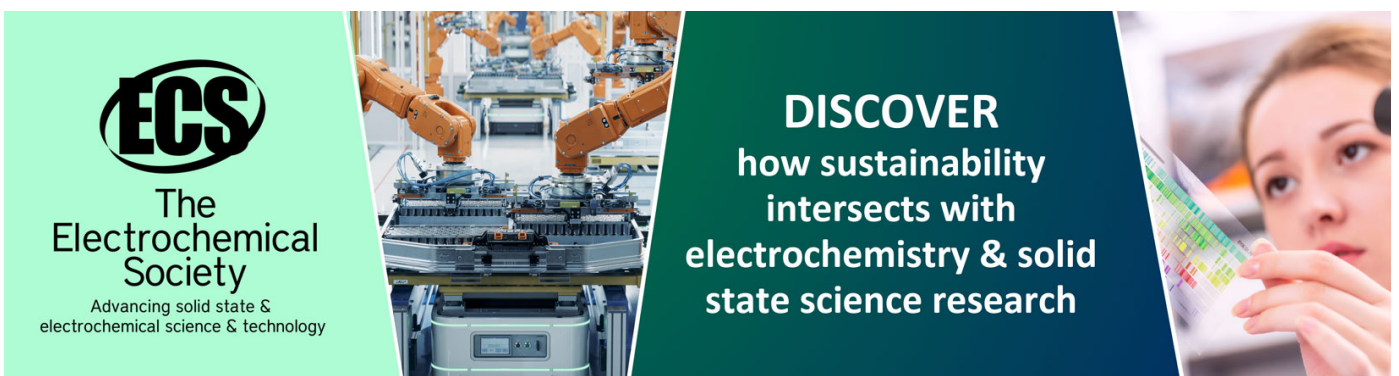
Improve the Performance of Porous Silicon for solar application by the embedding of Lithium Oxide nanoparticle

To cite this article: Shahlaa M. Abd Al Hussan *et al* 2020 *IOP Conf. Ser.: Mater. Sci. Eng.* **928** 072142

View the [article online](#) for updates and enhancements.

You may also like

- [Measurement of Optical Constants of Wet Porous Silicon Using In Situ Photoconduction](#)
Bernard Gelloz, Hiroki Fuwa and Lianhua Jin
- [\(Invited\) Photo-Assisted Etching of Porous Silicon Nanostructures in Hydrofluoric Acid Using Monochromatic Light](#)
Bernard Gelloz, Hiroki Fuwa, Eiichi Kondoh et al.
- [Chemical stabilization of porous silicon for enhanced biofunctionalization with immunoglobulin](#)
Nelson Naveas, Vicente Torres Costa, Dario Gallach et al.



ECS
The
Electrochemical
Society
Advancing solid state &
electrochemical science & technology

DISCOVER
how sustainability
intersects with
electrochemistry & solid
state science research

Improve the Performance of Porous Silicon for solar application by the embedding of Lithium Oxide nanoparticle

Shahlaa M. Abd Al Hussan¹, Nabeel A. Bakr¹, Ahmed N. Abd^{2*}

Department of Physics, College of Science, University of Diyala, Diyala, Iraq¹;

Department of Physics, College of Sciences, Mustansiriyah University, Iraq²

shahlamn91@yahoo.com

E-mail : ahmed_naji_abd@uomustansiriya.edu.iq

Abstract. The present research concerns the manufacture of porous silicon (PSi) by means of electrochemical etching method at (10 mA.cm⁻²) current density and approximately 10 minute etching time. The porous silicone layer was investigated by XRD, AFM and FTIR, and then Li₂O nanoparticles (NPs) were prepared by a simple chemical method. And freshly embedding three drops of (Li₂O) solution using the drop casting technique on the 40°C porous silicon(n-Psi) method to produce the heterojunction Al / Li₂O / PSi / Al. The results of current-voltage (I-V) test showed that the solar cell 's maximum power conversion efficiency (PCE) was 2.49% and thus the fill factor was 66.12%. A diffusion of Li₂O NPs on PSi solar cell characteristics assures an improvement on their properties.

Keywords: Porous silicon, Li₂O NPs, Electrochemical etching, XRD, solar cell.

1. Introduction: Since the 1950s, Uhlir and Turner have recognized the formation of porous silicon in an anodizing setting as pioneering work at Bell Labs[1, 2]. But it took more than 30 years to invent an electrochemical drilling process by Lyman and Bean to produce arrays of large pores arranged in silicone[3]. Other groups followed, and this new subject was developed in materials science as an significant field. The silicone pattern thus covers several times in size the "growth" of the pores in the silicon. Structures with pores below a small nanometer are considered nanometers, according to the IUPAC nomenclature for porous materials[4]. Its formation must be mechanically described by quantum[5]. Medium structures range between 2 and 50 nanometres. The bigger follicle is termed the big follicle. The pore morphology obtained depends on the properties of silicon (stimulants, resistance, orientation), electrolyte composition (organic, organic and concentration), and external parameters such as temperature, voltage, and lighting. Besides several review articles that can be found in the literature (for example [6-8]). Large structures etched into an aqueous solution of hydrofluoric acid (HF) allow us to specifically design sample parameters among the different methods of making porous silicone. This method developed an understandable and applicable instrument for the manufacture of devices and molds. One important feature is the possibility of producing arranged pore arrays of



specific diameters and lengths. The diameters of Pore can be varied between several hundred nanometers and the several micrometres. Curiously, a few hundred micrometers deep may be digged to the pores. So you can get the dimensions of 500:1 and more without loss Pore structure and form. The basic mechanisms for creating large pores in silicone will then be discussed more in detail below, this objective of this work is to prepare a PSI, thus it is included by Li_2O NP to improve the porous silicone porous cell 's efficiency.

2. Experimental work

2.1. Fabricate of porous silicon

Electrochemical etching was used to produce porous silicon(n-PSi) that used a silicon wafer substratum with an electrolyte Teflon cell that contains about 43 percent(HF) acid and 99.9percent pure ethanol with volume 1:1, as seen in Figure 1. The sample made from monocrystalline silicone was treated with a $10 \Omega \cdot \text{cm}$ resistance and direction (100) direction. The chemical treatment for n-Psi was to generate a guard using current $10 \text{ mA} \cdot \text{cm}^{-2}$ at 10 minutes, and then the wafer's back side was deposited at 10^{-5} Torr vacuum around (200 μm) thick aluminum back contact.

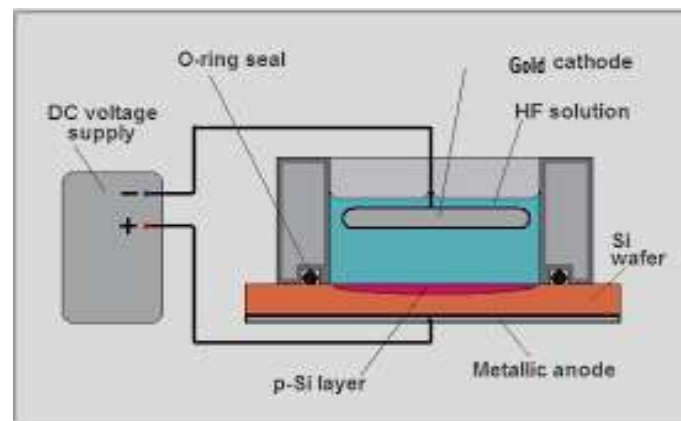


Fig. 1: Electrochemical etching set-up scheme diagrams.

2.2. Prepare of Li_2O nanoparticles by simple chemical method

Li_2O NPs has been produced by a method of chemical precipitation. A standard procedure dissolved 0.6 grams of Lithium Powder (MART India) in 100 ml volumetric flask. The solution was applied with a stirring into a round-bottom glass bottle. The mixture was white in colour. Lithium oxide (Li_2O) depositing on the glass substrate using a drop-casting process, seen Figure (2).The solution of (Li_2O) was deposited at 40°C on pre - heated transparent conductive porous silicon(n-type) by the same method, time sintering time is 1 minute. The thin film thickness was calculated by weight method for the lithium oxide, and the thin film thickness would be about (250 nm).

2.3. Fabricate of Al/ Li_2O /PSi/n-Si/Al Heterojunction

Drop-casting deposited Li_2O 's precursor solution was impregnated with hot substrate porous silicon (n-type) at 40°C as Three drops to produce an Al / Li_2O / PSi / Si / Al heterojunction for solar cells, a hot substrate was left to cold at room temperature. And place foil Al with area 0.1 cm^2 as electrodes on the layer Li_2O / PSi / n-Si, as can be seen in Figure 2.

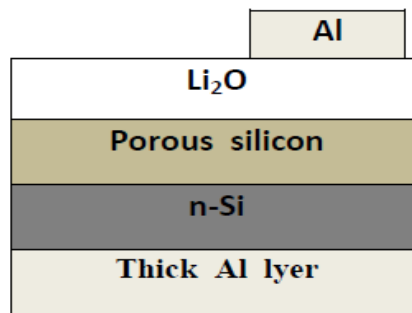


Fig. 2: The basic structure of typical Al/ Li_2O /PSi/n-Si/Al heterojunction

3.The Results

3.1. XRD measurement

The X-ray diffraction patterns for the synthesized's crystalline nature (n-PSi and Li_2O) are illustrated through Figure(3). By comparison with JCPDS No. 74-6256, it can be noted from this figure that the XRD patterns match the Li_2O powders value. All diffraction peaks of prepared thin film exhibit Rhombohedra structure, and the Li_2O thin film structure has a secondary phase. This peak is assigned by (♦) in figure(1a). This diffraction peak attributed to Li_2O_2 phase by comparison with JCPDS No. 73-1640. The phase (♦) has been hexagonal structure. The average crystallite size for the film is calculated by Scherrer's formula by using the Eq.(1)[9]. Where (D) is the crystallite size, (λ) is the wavelength (1.5406\AA) of X-ray, (θ) is the diffraction angle, and (β) is the full width at half maximum (FWHM). The crystallite size of (n-PSi and Li_2O) indicates that the size of the prepared samples would be within the nanoscale as seen in Table(1). The micro strain value(η) and also the dislocation density(δ) have been determined from Eq(2,3):

$$D = \frac{0.9\lambda}{\beta \cos(\theta)} \quad (1)$$

$$\eta = \frac{\beta \cos \theta}{4} \quad (2)$$

$$\delta = \frac{1}{D^2} \quad (3)$$

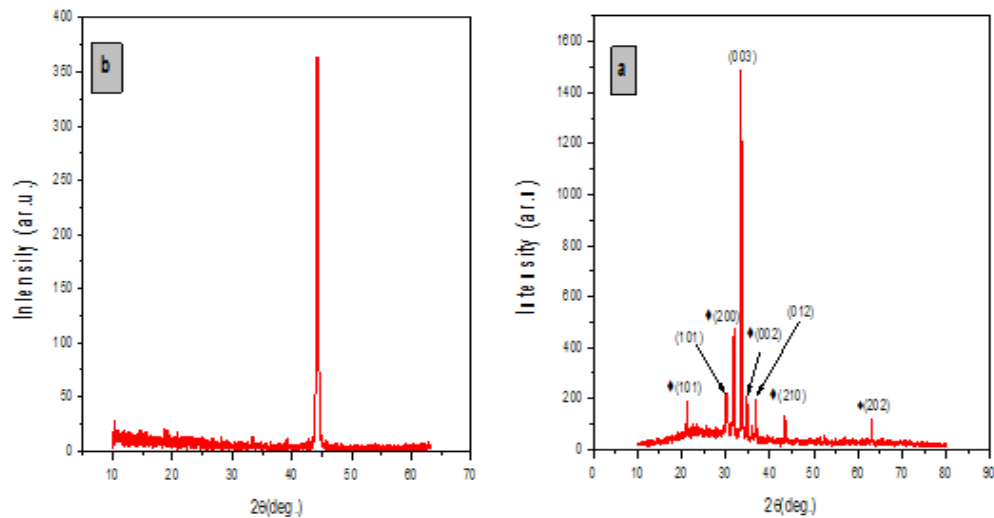


Fig. 3:The XRD patterns of (a): n-Psi, (b): Li₂O nanoparticle.

Table 1: Summary of X-ray characterization

Sample	2 θ (deg)	D(nm)	$\delta \cdot 10^{14}$ (lin.m ⁻²)	$\eta \cdot 10^{-4}$ (lin.m ⁻⁴)
n-PSi	44.2371	28.81	12.04	0.1203
Li ₂ O	30.3195	45.6	4.809	7.600
	33.5130	35.2	8.07	9.820
	36.8438	52.06	3.689	6.657
Li ₂ O ₂	21.2907	36.84	7.366	9.407
	31.8811	51.92	3.709	6.675
	34.7814	45.76	4.774	7.574
	43.4709	51.56	3.761	6.538
	63.0207	66.87	2.235	5.182

3.2. Atomic force microscopy (AFM)

AFM is a device used for studying the shape and texture of various surfaces. This approach allows the monitoring of diversity and the assessment of the sample's exact morphological properties, suggesting better facilities than most other microscopic methods. In 3D surface scanning of AFM, a image analysis allows selection; tends to give the mean root square roughness, the average particle height and periodicity intensity spectra throughout the order of particles[10,11].The properties, including the roughness, porosity, medium size and particle size distribution, that influence the optical, electrical, mechanical, and magnetic properties of the sample surface can be evaluated using appropriate software. Figure(4: a) shows the (3D) AFM images and also the distribution of Li₂O film granular cumulation. That film was made with a highly dispersed disk, and also the grains are homogeneous and aligned parallel. Figure(4: b) clearly shows the (3-D) AFM images and thus the distribution chart of a n-PSi. AFM image shows also that pores were distributed uniformly within in the scanning area(500x500 nm) with individual column pores extending wards. The average grain size for pore was calculated by AFM analysis using specialized software that was observed to be approximately 65.25

nm based on processing conditions (current density of 10 mA / cm² and 10 minute etching time). That atomic force microscope images provided information on surface roughness morphology, root mean square (RMS) and thin film roughness density as seen in Table(2).The surface roughness can all be calculated from the root mean square (RMS), which is known as that of the standard deviation of surface height from average height. Surface roughness is measured by calculating the standard deviation for so many curves or curve averages of surface irregularities.

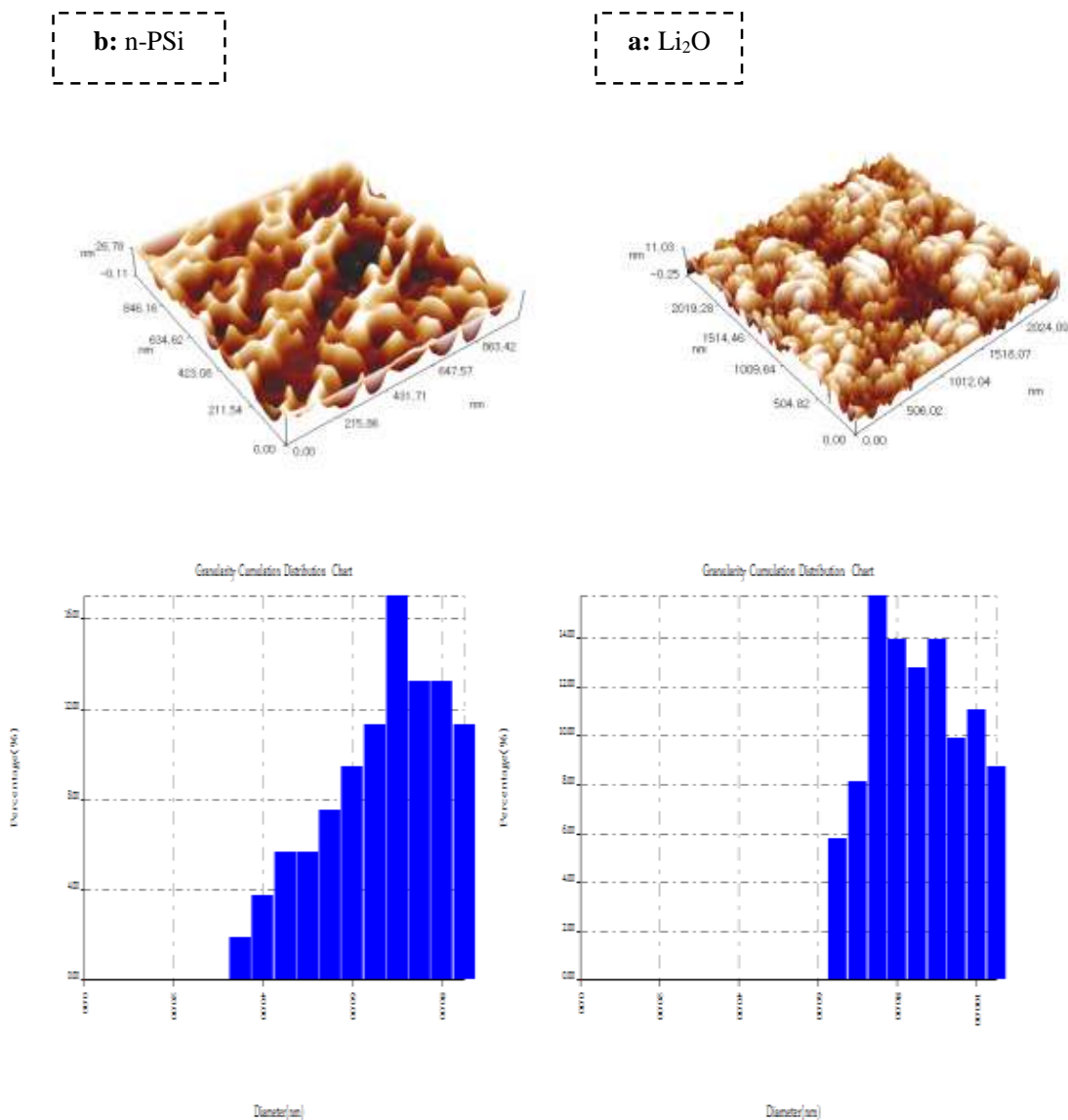


Fig. 4:Shows (a) 3D AFM image and (b) Distribution of granular accumulation chart.

Table 2: Average grain size, roughness surface and Root mean square (RMS)

Sample	Average grain size (nm)	Roughness average (nm)	Root mean square (nm)
n-PSi	65.25	6.73	7.77
Li₂O	83.19	2.59	3.03

3.3. Optical properties

Figure (5) displays the optical transmittance on Li₂O thin film, that transmittance reaches its maximum value around (>70%) at UV wavelength (260 and 330) nm and increases gradually above that, that's the feature for high transmitting nanoparticles at some of these wavelengths, while increasing the transmission as wavelength increases[12]. The change in transmittance as a function of wavelength of a Li₂O nanoparticles and also the increase in UV-Vis at 330-800 nm indicate the presence of using Li₂O nanoparticles in reagent and solar cell manufacturing[13]. Figure (6) shows the optical absorption coefficient for Li₂O thin film as a function of the photon energy. It can be shown that Li₂O thin film does have an absorption coefficient value of $\alpha > 10^5$ 1/cm that suggests an improvement in the probability of direct transitions occurring. It has been noted that the prepared thin film has a high absorption coefficient about the visible range of $\sim(1.5 \cdot 10^5)$ 1/cm in and the near-IR spectral range that is in agreement with the other reports[14]. By using the following equation[15], the optical band gap energy (E_g) of the Li₂O can be determined by Tauc's relationship of $(\alpha h\nu)^2$ versus photon energy (eV).

$$(\alpha h\nu) = A(h\nu - E_g)^n \quad (4)$$

Where n is 0.5 for the direct allowed transition, α is the absorption coefficient, A is the constant sharpening of the band edge, h is the Plank's constant and $h\nu$ is the photon energy. The optical band gap energy has been calculated by plotting $(\alpha h\nu)^2$, by extrapolating the linear portion of the plot to = 0. Figure (7) shows Tauc's Li₂O thin film plot plotting the square graph $(\alpha h\nu)^2$ versus the photon energy ($h\nu$). The value of the Li₂O thin film band gap is found to be roughly 5.33 eV.

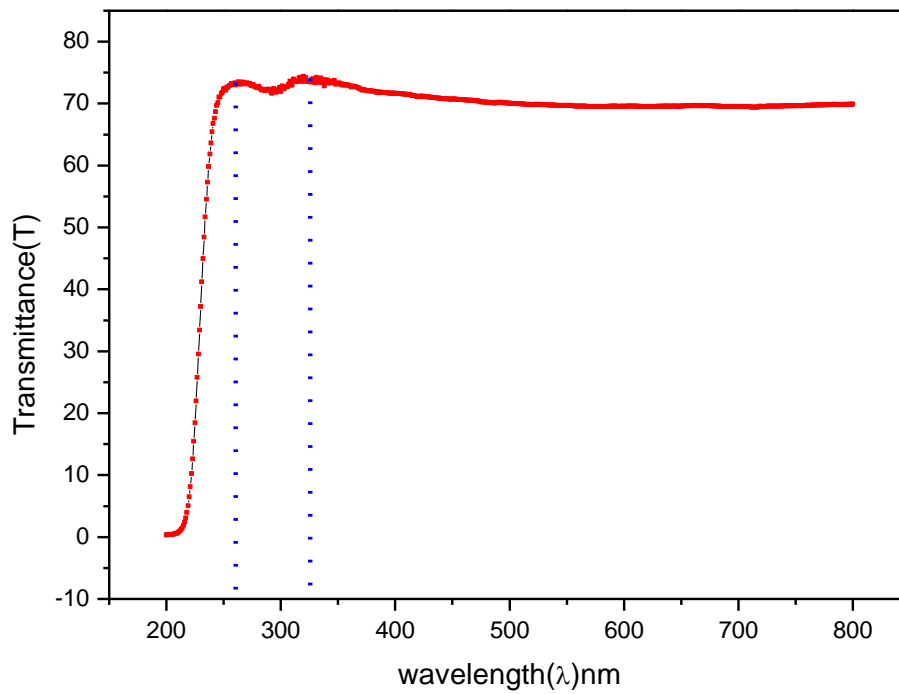


Fig. 5 :UV-Visible transmission spectrum of Li₂O thin film.

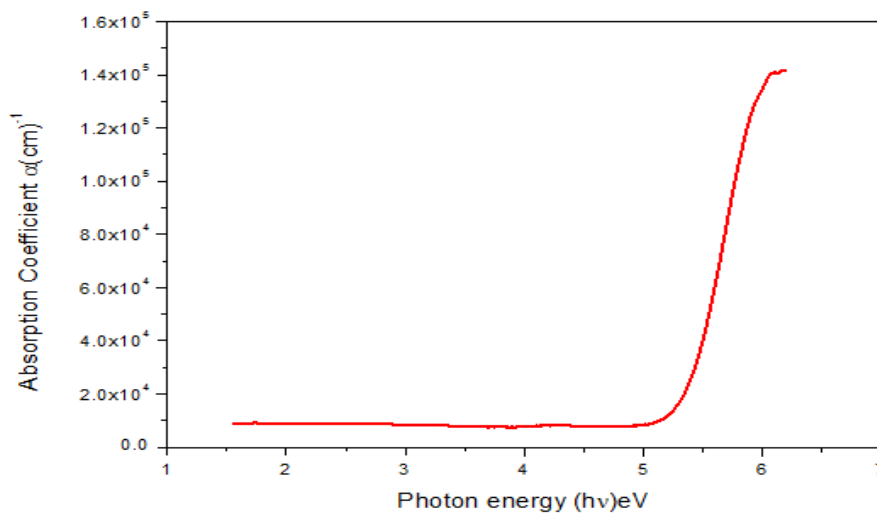


Fig. 6:Absorption coefficient versus photon energy for Li₂O thin film.

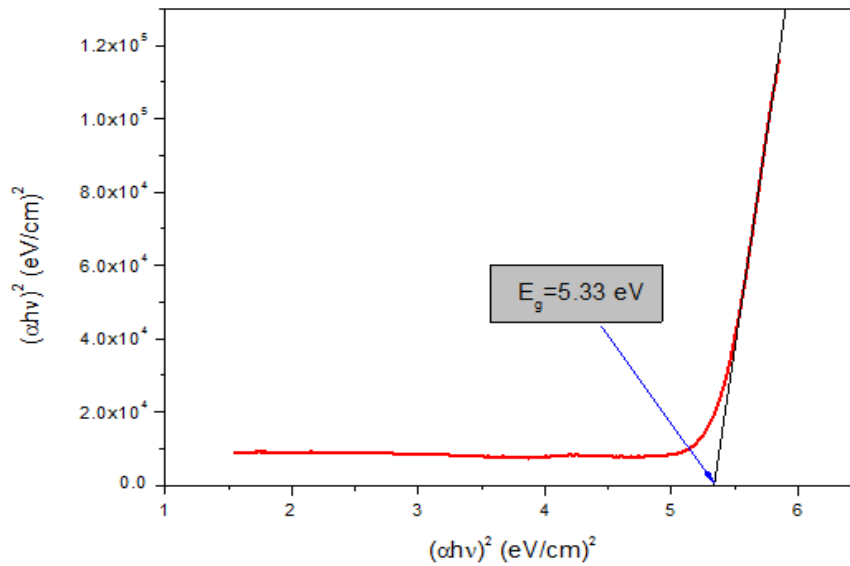


Fig. 7 :Tauc's plot of Li₂O thin film.

Due to the vast possibilities for technological application, the characteristics of visible photoluminescence (PL) in porous silicone layers (PSLs) have given an important impulses to material studies. The PSL studies aimed at increased stability of PL over long periods Initial work on PSLs is primarily aimed at identifying the sources of the mechanisms for radiative recombination. PL spectrum of a PSi / n-Si heterojunction formed at current density $(10) \text{ mA cm}^{-2}$ and 10 minute etching time as seen in the figure (8), shows an emission peak of 671 nm for n-PSi and an emission of 500 nm for fixed excitation wavelength. PL is pronounced in the 1.847 electron Volt spectral band, and this can be due to the luminescence from the restricted silicone structures accepted with these results[16].

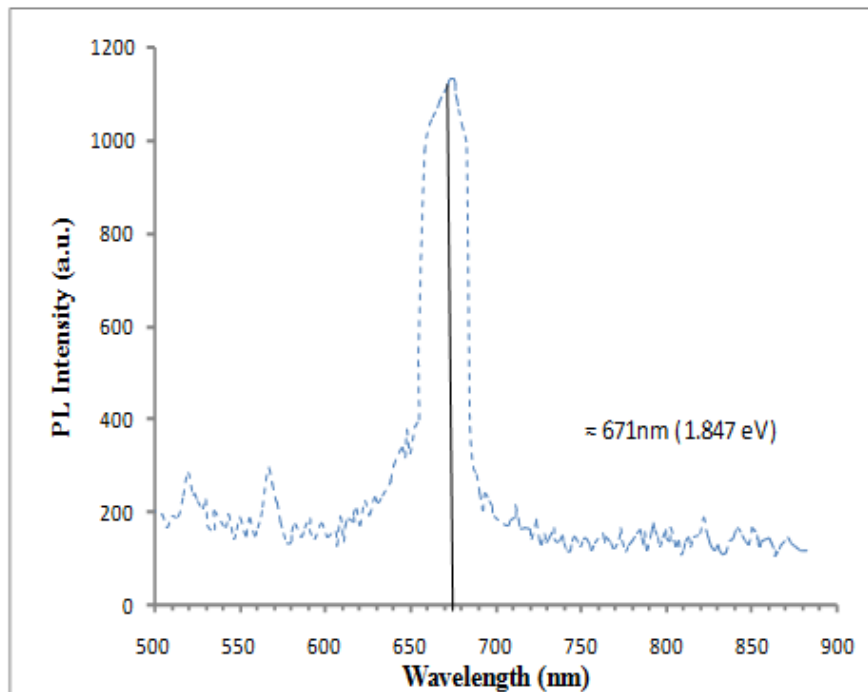


Fig. 8: PL spectra for n-PS

3.4. FT-IR spectra

Figure (9:a) shows the Li_2O powder FT-IR spectrum which was prepared using simple chemical method. The bands that appear at $(706.83) \text{ 1/cm}$ are caused by inter-atomic vibrations correspond to (Li-O-Li). Noticed the $(1625.91 \text{ and } 3449.37) \text{ 1/cm}$, possibly due to expansion and deform deformation of (O-H). The bands correspond for (O_4) showed up at $(900.69) \text{ 1/cm}$ and $(1044.34) \text{ 1/cm}$ for (O_3) , respectively to absorb water on the metal surface. Kurnar and Rani reported that similar FT-IR spectra were observed in Li_2O , which would be a high-profile film[17]. PSi surface chemical composition can be tested with FTIR spectroscopy successfully. The FTIR spectrum for n-PSi layer was indicated by Figure (9:b) By FTIR data for n-PSi, it can be noted that the main peak was in the range about $(1037.54\text{-}828.93) \text{ 1/cm}$ that was due to the presence of (Si-O-Si) wagging because the range $(2099.65) \text{ 1/cm}$ was according to (Si-H)wagging mode, peak at 664.46 1/cm noticed, due to (Si-O). A small peak at $(2925.44) \text{ 1/cm}$ may be attributed to angle deformation (C - H). The $(1569.03) \text{ 1/cm}$ may be observed, probably due to expansion and deformation (O-H). Even so, since carbon and silicon are on the same periodic table board, there's also a possibility that the carbon atom will replace a siliconatom[18].

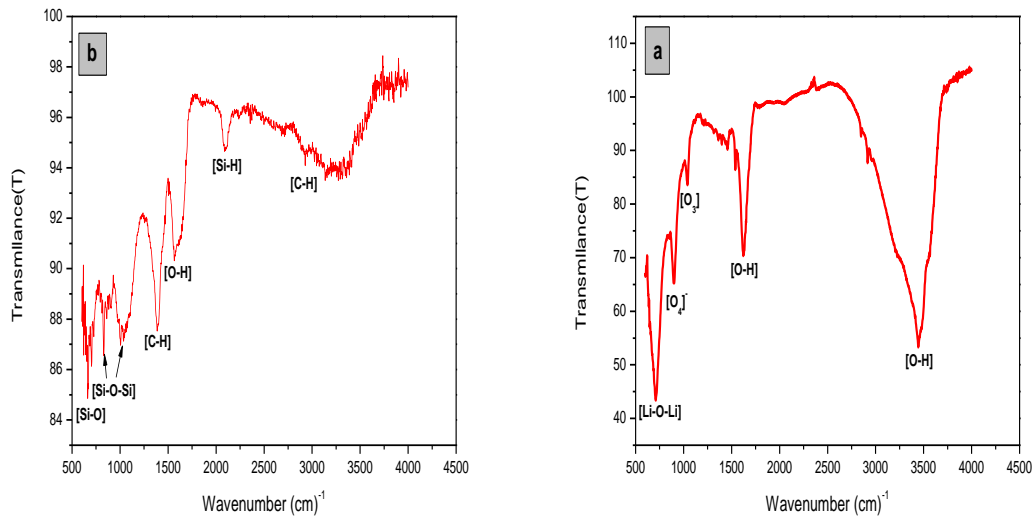


Fig. 9: FTIR of (a):Li₂O nanoparticle, (b): n-Psi.

3.5. SEM

Figure(10) displays SEM images prepared by simple chemical method, with two magnifications of Li₂O NPs. It can be certain in the SEM images that these NPs have different morphologies. It has been noted that Li₂O NPs morphology is not uniform and is made up of several tiny irregular nanoparticles.

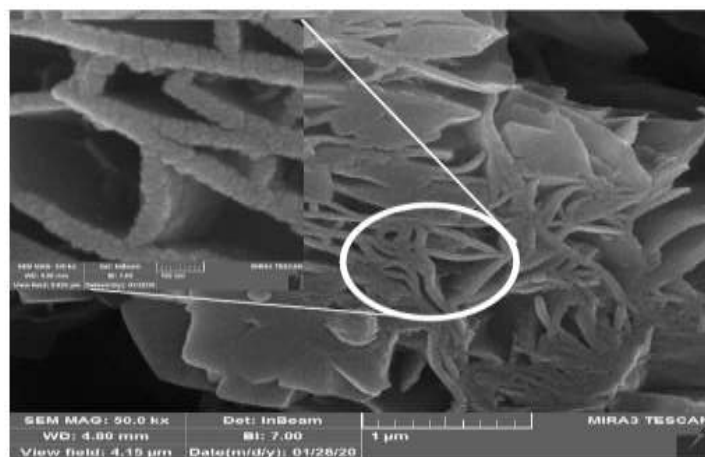


Fig. 10: SEM micrographs of the Li₂O thin films

3.6. Li₂O /n-PSi Heterojunction Solar cell properties

Figure(11) shows that the particles of Li_2O are deposited on the surface of silicon by the drop casting method only (5) drops and then dry at 80°C to make the $\text{Li}_2\text{O}/\text{Si}$ solar cell. I-V dark characteristics of Al / Li_2O / n-Si / Al Solar Cells in forward and reverse direction. Solar cell's forward current is very small at voltages less than 2 V. This current is called recombination current and only occurs at low voltages. This is produced when each electron excited the conductive band to form valence band. The second high voltage region represented the region of diffusion or binding which depends on the serried resistance. The bias voltage can deliver electrons with sufficient energy in this region to penetrate the barrier between the two sides of the junction.

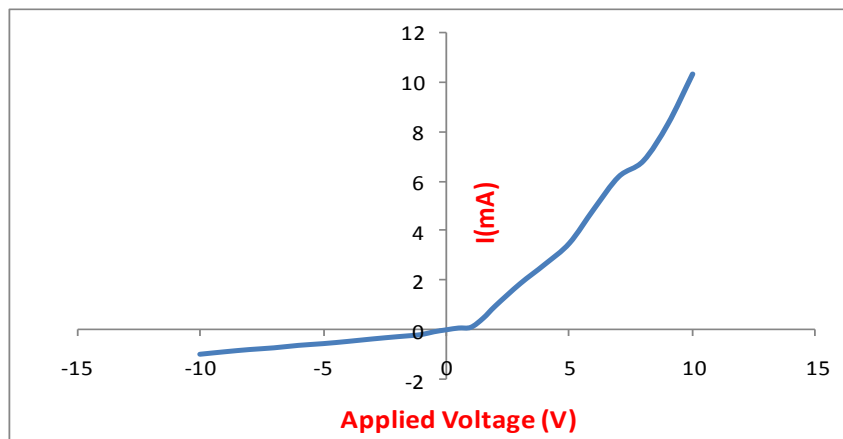


Fig. 11: (I-V) in the dark characteristics for both reverse and forward bias of the $\text{Li}_2\text{O}/\text{Psi}$ heterojunction.

Figure(12) demonstrates that the Al / Li_2O / PSi / Si / Al bright (current-voltage) characteristics producing photocurrent under a 10mWm^{-2} tungsten lamp illumination. It has been shown that the reverse current value for the Li_2O / n-Si heterojunction under illumination at a given voltage is higher than that in the dark which indicates that, as a result of light absorption, the light generated carrier – contributing photocurrent as a result of electron – hole production. Such behavior yields useful information about the pairs of the electron-hole that are effectively produced by incident photons in the junction.

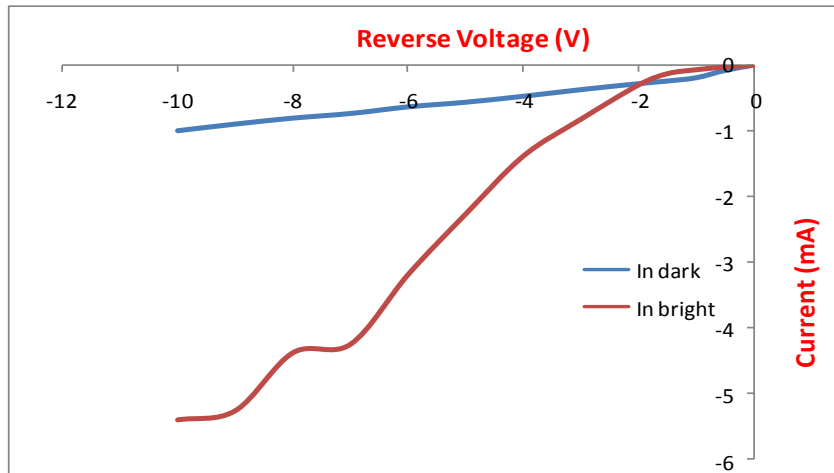


Fig.12: (I–V) characteristics for forward and reverse biasing applied to $\text{Li}_2\text{O}/\text{PSi}$ with illumination.

Figure(13) Shows the I-V curve for $\text{Li}_2\text{O}/\text{n-Si}$ heterojunction. Equations(5) and (6)[19]

$$\mathbf{FF(\%)} = \frac{J_{\max}V_{\max}}{J_{sc}V_{oc}} = \frac{P_{\max}}{J_{sc}V_{oc}} \times 100\% \quad (5)$$

$$\mathbf{\eta(\%)} = \frac{J_{\max}V_{\max}}{P_{in}} = \frac{P_{\max}}{P_{in}} = \frac{J_{sc}V_{oc}}{P_{in}} \mathbf{FF} \times 100\% \quad (6)$$

The measured short-circuit current, open-circuit voltage, filling factor and efficiency were calculated respectively by $1.2\mu\text{A}$, 24.7 mV , 66.12 and 2.49 percent. All of the results indicate relief that the $\text{Li}_2\text{O} / \text{n-Si}$ sandwich structure could be used as a solar[20].

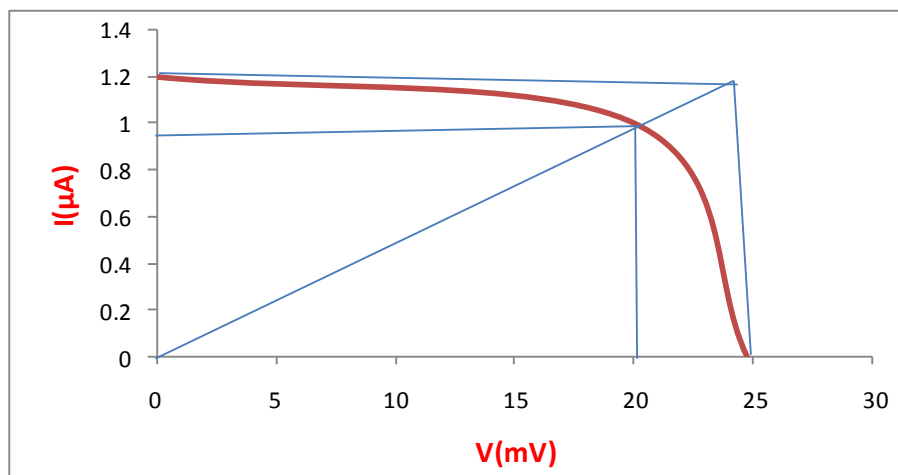


Fig.13: (I-V) curve of $\text{Li}_2\text{O}/\text{n-Si}$ solar cell

4. Conclusions

The XRD results showed that the Li₂O films with preferred orientation along (003) direction are nanocrystalline. The Li₂O thin film synthesized was in 35.2 nm nanosized, which was prepared by chemical method. X-ray diffraction (XRD) measurements indicate that Li₂O particle was polycrystalline with Rhombohedra crystal structure and there was a hexagonal structure in the secondary phase (♦) of the Li₂O thin film. (SEM) showed that Li₂O was a ball-shaped particle. The optical properties showed that the Li₂O thin film with direct band gap was 5.33 electron Volt. By simple chemical method, the Li₂O / PSi / n-Si heterojunction was successfully manufactured using electrochemical silicon etching and the deposition of Li₂O thin films. Li₂O shows good transparency throughout the wavelength range (200-800) nm, and the heterojunction electrical characteristics were strongly dependent on the structure. Si porosity has improved the performance of the heterojunction Li₂O / PSi / n-Si to become very effective materials for solar cell applications

References

- [1] D. R. Turner 1958 Electro polishing Silicon in Hydrofluoric Acid Solutions *J. Electrochem. Soc.*, 105 (7) 402–408.
- [2] A. Uhlir 1956 Electrolytic Shaping of Germanium and Silicon *Bell System Tech. J.*, 35 333–347.
- [3] V. Lehmann and H. Föll, 1990 Formation Mechanism and Properties of Electrochemically Etched Trenches in n-Type Silicon *J. Electrochem. Soc.*, 137(2) 653–659 .
- [4] D. H. Everett. IUPAC 1972 Manual of Symbol and Terminology for Physicochemical Quantities and Units, Appendix, Definitions, Terminology and Symbols in Colloid and Surface Chemistry *Part I. Pure Appl. Chem.*, 31(4) 577.
- [5] V. Lehmann and U. Gösele 1991 Porous silicon formation: A quantum wire effect *Appl. Phys. Lett.*, 58(8) 856–858.
- [6] H. Föll, M. Christophersen, J. Carstensen and G. Hasse 2002 Formation and application of porous silicon *Mater. Sci. Eng. R*, 39(4) 93–141.
- [7] X. G. Zhang 2004 Morphology and Formation Mechanisms of Porous Silicon *J. Electrochem. Soc.*, 151(1) C69–C80.
- [8] V. Lehmann 2002 Electrochemistry of Silicon: Instrumentation, Science, Materials and Applications *Wiley-VCH Verlag GmbH*.
- [9] L.-C. Chen, C.-Y. Weng 2015 Optoelectronic properties of MAPbI₃ perovskite/ titanium dioxide heterostructures on porous silicon substrates for cyan sensor applications *Nanoscale Res. Lett.* 10 (1) 404.

- [10] S.K. Shrama, N. Saurakhiya, S. Barthwal, R. Kumar, A. Sharma 2014 Tuning of structural, optical, and magnetic properties of ultrathin and thin ZnO nanowire arrays for nano device applications *Nanoscale Res. Lett.* 9 (1) 1-17.
- [11] Nabeel A. Bakr et al 2015 Effect of Substrate Temperature on Structural and Optical Properties of Cu₂ZnSnS₄ (CZTS) Films Prepared by Chemical Spray Pyrolysis Method *Research Journal of Chemical Sciences* 5(10) 51-61 October
- [12] T. Defforge et al 2012 Plasma-deposited fluoropolymer film mask for local porous silicon formation *Nanoscale Res. Lett.* 7 1-8.
- [13] S.K. Shrama et al 2014 Tuning of structural, optical, and magnetic properties of ultrathin and thin ZnO nanowire arrays for nano device applications *Nanoscale Res. Lett.* 9 (1) 1-17.
- [14] J D Wolfe and N L Thomas 2000 Durable silver coating for mirrors *US Patent* 6078(6) 25.
- [15] Wang, Z. et al 2002 Low-temperature synthesis of ZnO nanoparticles by solid-state pyrolytic reaction *Nanotechnol.* 14 1-11.
- [16] A. Khaldun Salman et al 2012 Effect of Silicon Porosity on Solar Cell Efficiency *Int. J. Electrochem. Sci.* 7 376-386.
- [17] Sun, X. W. and Kwok, H.S 1999 Optical Properties of Epitaxially Grown Zinc Oxide Films on Sapphire by Pulsed Laser Deposition *J. Appl Phys.* 86 408-411.
- [18] Xuefeng Wang and Lester Andrews 2009 Infrared spectra, structure and bonding in the LiO₂, LiO₂Li, LiO and Li₂O molecules in solid neon *Molecular Physics* 107(8-12) 739-748.
- [19] Kumar, H. and R. Rani 2013 Structure and optical characterization of ZnO nanoparticles synthesized by microemulsion route *Intl. Lett, Chem. Phys, Astron.* 14 26-36.
- [20] Ahmed N. Abd et al 2018 Improve the photo response of porous silicon for solar cell applications by embedding of CdTe *Surface Review and Letters* 25(2) 1850012.
- [21] M.H. Suhail and A.M. Jafar 2016 Fabrication and characterization of organ lead halide peroviskesolar *Elixir Renew. Energy* 98 42709-42713.